9.8 TURBULENT PRESSURE STATISTICS

Natasha L. Miles, John C. Wyngaard,* and Martin J. Otte

Department of Meteorology, The Pennsylvania State University
University Park, Pennsylvania 16802

1. INTRODUCTION

Although the turbulent pressure field is extremely important in turbulence dynamics, it has not been studied as extensively as other fields, in part due to the inherent difficulty of its measurement. We use large-eddy simulation (LES) to calculate resolvable-scale turbulent kinematic pressure (i.e., the resolvable pressure divided by the density) fields and their wavenumber (κ) spectra in two convective atmospheric boundary layers: a free convection case with zero mean horizontal wind speed and a convective case in which the mean wind speed is nonzero, being set at 15 m s^{-1} above the boundary layer. In each case the LES domain is 2500 m square in the horizontal and 1000 m deep. The capping inversion height, z_i, is about 600 m. The LES code uses 140 × 140 Fourier modes in the horizontal plane and 160 grid points in the vertical direction.

2. PRESSURE SPECTRAL CONSTANTS

Turbulence spectra in the observational community, in traditional turbulence analysis, and in this analysis all differ—a source of possible confusion. The observational community can usually obtain only one-dimensional spectra along the mean-wind direction. Traditional turbulence analysis often assumes isotropy and integrates over constant-wavenumber spherical shells in three-dimensional wavenumber space to obtain what are called three-dimensional spectra. Our LES flow is homogeneous only in the horizontal, so we integrate over constant-wavenumber rings in the horizontal plane to obtain what we call two-dimensional spectra. We shall now relate the two-dimensional spectrum of kinematic pressure p/ρ first to its three-dimensional spectrum and then to its one-dimensional spectrum, following Wyngaard (2002).

The integral of the pressure spectrum $\phi(\boldsymbol{\kappa})$ over spherical shells in three-dimensional κ-space gives what is called its three-dimensional spectrum. Under the assumption of isotropy, $\phi(\boldsymbol{\kappa}) = \phi(\kappa)$ and the three-dimensional pressure spectrum $E(\kappa)$ is

$$E(\kappa) = 4\pi\kappa^2\phi(\kappa). \tag{1}$$

Using Kolmogorov scaling, Lumley and Panofsky (1964) predicted the behavior of the three-dimensional pressure spectrum in the inertial subrange. They assumed that $E(\kappa)$ depends only on the rate of viscous dissipation per unit mass, ϵ, and wavenumber, κ, from which it follows that

$$E(\kappa) = a_3\epsilon^{4/3}\kappa^{-7/3}, \tag{2}$$

with a_3 a presumably universal constant. This result was more recently found by Hill and Wilczak (1995) by analytical means.

Our LES flow is homogeneous only in the horizontal plane with a pressure spectrum $\phi_h(\kappa_1, \kappa_2)$. If the flow is isotropic as well, ϕ_h depends only on the horizontal wavenumber magnitude, κ_h, where $\kappa_h^2 = \kappa_1^2 + \kappa_2^2$, and ϕ_h can be written as

$$\phi_h(\kappa_h) = \int_{-\infty}^{\infty} \phi(\kappa) d\kappa_3. \tag{3}$$

Using Eqs. (1), (2), and (3), we have

$$\phi_h(\kappa_h) = \int_{-\infty}^{\infty} \frac{a_3}{4\pi}\epsilon^{4/3}\kappa^{-13/3} d\kappa_3. \tag{4}$$

The counterpart of $E(\kappa)$ in the plane is $E_h(\kappa_h)$, the integral of ϕ_h over circular rings. We call E_h the two-dimensional pressure spectrum. Under isotropy in the plane it becomes simply

$$E_h(\kappa_h) = 2\pi\kappa_h\phi_h(\kappa_h). \tag{5}$$

Using Eqs. (4) and (5), we have

$$E_h = \frac{a_3}{2}\epsilon^{4/3}\kappa_h \int_{-\infty}^{\infty} \kappa^{-13/3} d\kappa_3. \tag{6}$$

After variable changes, Eq. (6) becomes

$$E_h = a_3\epsilon^{4/3}\kappa_h^{-7/3} \int_0^{\pi/2} (cos\theta)^{7/3} d\theta, \tag{7}$$

where θ is the angle between $\boldsymbol{\kappa}$ and $\boldsymbol{\kappa_h}$. The integral in Eq. (7) can be expressed in terms of Gamma functions and then Eq. (7) simplifies to:

$$E_h = 0.74\, a_3\epsilon^{4/3}\kappa_h^{-7/3}. \tag{8}$$

*Corresponding author address: John C. Wyngaard, Department of Meteorology, The Pennsylvania State University, 503 Walker Building, University Park, PA 16802; e-mail: wyngaard@ems.psu.edu

If we write the two-dimensional spectrum in the inertial subrange as

$$E_h = a_2 \epsilon^{4/3} \kappa_h^{-7/3}, \tag{9}$$

and use Eq. (8), we then have the relationship between the two- and three-dimensional spectral constants

$$a_2 = 0.74\, a_3. \tag{10}$$

Experimentalists measure the one-dimensional spectrum of pressure, $F(\kappa_1)$. Under isotropy it is the integral of $\phi_h(\kappa_h)$ over all κ_2:

$$F(\kappa_1) = 2 \int_{-\infty}^{\infty} \phi_h(\kappa_h) d\kappa_2. \tag{11}$$

The factor of two in Eq. (11) is required so that F integrates over the half-line to the variance, as is customary in experimental micrometeorology. In the inertial subrange this becomes, using Eqs. (5), (9), and (11),

$$F(\kappa_1) = 2 \int_{-\infty}^{\infty} a_2 \epsilon^{4/3} \kappa_h^{-10/3} d\kappa_2. \tag{12}$$

Solving in a manner similar to the two-dimensional case, we find

$$a_1 = 0.58\, a_2, \tag{13}$$

where we have used the definition of the one-dimensional spectrum in the inertial subrange:

$$F(\kappa_1) = a_1 \epsilon^{4/3} \kappa_1^{-7/3}. \tag{14}$$

3. PRESSURE RETRIEVAL

The LES code solves the filtered equation of motion

$$\frac{\partial u_i^r}{\partial t} + \frac{\partial u_i^r u_j^r}{\partial x_j} + \frac{\partial \tau_{ij}}{\partial x_j} = -\frac{\partial p^r}{\partial x_i} - 2\epsilon_{ijk}\Omega_j u_k^r + \frac{g\delta_{i3}}{\theta_0}\theta^r, \tag{15}$$

subject to the continuity condition

$$\frac{\partial u_i^r}{\partial x_i} = 0, \tag{16}$$

where u_i^r is the filtered or *resolvable* fluctuating velocity field, p^r is the resolvable kinematic pressure, Ω_j is the earth's rotation vector, θ_0 is the background, adiabatic profile of potential temperature, g is the acceleration of gravity, and θ^r is the resolvable-scale fluctuating potential temperature. This equation incorporates the usual Boussinesq treatment of buoyancy. Because of the large Reynolds number of atmospheric boundary layer flow, the filtered viscous term is negligible and so does not appear. The term $\tau_{ij} \equiv (u_i u_j)^r - u_i^r u_j^r$ is the subgrid-scale kinematic stress that originates through the filtering of the nonlinear advection term in the equation of motion.

The LES code solves Eq. (15) numerically, using periodic boundary conditions in the horizontal directions and finite differences in the vertical direction (Moeng 1984). Taking the divergence of Eq. (15) gives a Poisson equation for the resolvable kinematic pressure field for quasi-steady conditions (Moeng and Wyngaard 1986):

$$\nabla^2 p^r = -\left(2\frac{\partial u_i^{r\prime\prime}}{\partial x_j}\frac{\partial U_j}{\partial x_i} + \frac{\partial u_i^{r\prime\prime}}{\partial x_j}\frac{\partial u_j^{r\prime\prime}}{\partial x_i}\right) - \frac{\partial^2 \tau_{ij}}{\partial x_i \partial x_j} - 2\epsilon_{ijk}\Omega_j \frac{\partial u_k^r}{\partial x_i} + \frac{g}{\theta_0}\frac{\partial \theta^r}{\partial z}. \tag{17}$$

We break the divergence of the advection term in Eq. (15) into two parts: the first term on the right-hand side of Eq. (17) is the mean-shear contribution and the second term is turbulent-turbulent contribution. Here U_j is the horizontal average of u_j and a double prime denotes a deviation from the horizontal average.

Solving Eq. (17) with the appropriate upper and lower boundary conditions yields the resolvable-scale kinematic pressure field, $p^r(x, y, z, t)$ at each time step. We use the pressure solver discussed by Moeng and Wyngaard (1986) to isolate the contributions from each of the terms on the right side. That is, we write

$$p^r = p^{ms} + p^{tt} + p^{sg} + p^c + p^b, \tag{18}$$

so that the resolvable pressure is the sum of mean-shear, turbulence-turbulence, subgrid, Coriolis, and buoyancy contributions, respectively. We accomplish this with the solver in the LES code, in turn zeroing all but one of the forcing terms on the the right side of Eq. (18), using the appropriate boundary conditions for that component, and solving for each component of pressure. This ensures that the numerics in the pressure-decomposition solver are precisely those of the pressure solver in the LES code.

We can also solve for the buoyancy and mean-shear contributions to the pressure spectrum analytically. We write a Poisson equation for the "buoyant pressure," p^b, the fluctuating kinematic pressure field driven solely by buoyancy. In the Boussinesq approximation this is

$$\nabla^2 p^b = \frac{g}{\theta_0}\frac{\partial \theta}{\partial z}. \tag{19}$$

It can be shown that this yields a relation between the resulting buoyant pressure spectrum and the temperature spectrum:

$$\phi_p^b(\boldsymbol{\kappa}) = \left(\frac{g}{\theta_0}\right)^2 \frac{\kappa_3^2}{\kappa^4} \psi(\boldsymbol{\kappa}), \tag{20}$$

where $\boldsymbol{\kappa}$ is the three-component wavenumber vector and ψ is the temperature spectrum. Assuming $\phi_p^b(\boldsymbol{\kappa})$ is isotropic in the horizontal plane and integrating over κ_3, the equation that relates the two-dimensional spectra in their inertial subranges is

$$E_h^b(\kappa_h) = C\left(\frac{g}{\theta_0}\right)^2 \kappa_h^{-11/3}. \tag{21}$$

C depends on the inertial-subrange level of the two-dimensional temperature spectrum E_h^θ:

$$C = 0.13\, \kappa_h^{5/3} E_h^\theta. \tag{22}$$

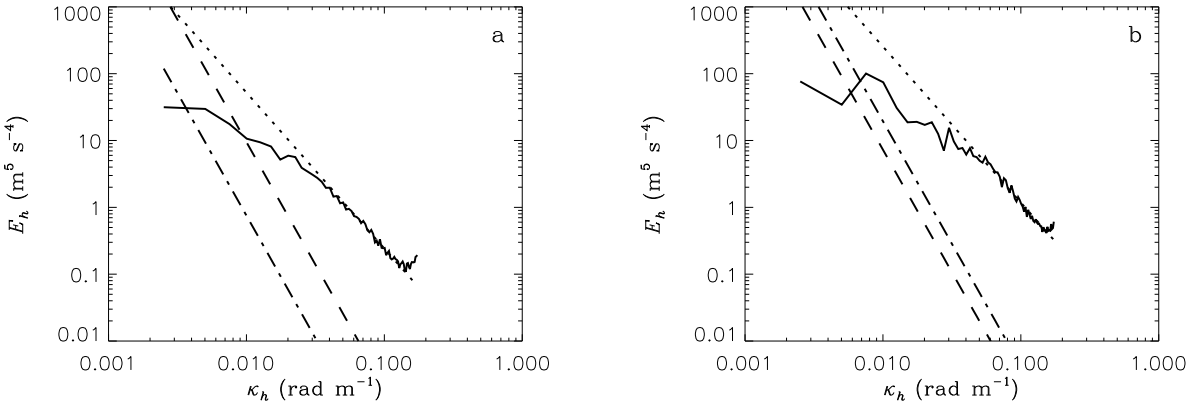

Figure 1: Two-dimensional pressure spectra at $z = 0.10\ z_i$ for a) free convection and b) convection with shear. The dotted line is the $-7/3$-slope line that best fits the pressure spectrum in the inertial subrange. The dashed line is the analytical solution for the buoyancy contribution to the pressure spectrum and the dot-dashed line is the analytical solution for the mean-shear contribution to the pressure spectrum.

We determine the mean-shear contribution in a similar manner. The poisson equation for the mean-shear part of the fluctuating pressure is given by

$$\nabla^2 p^{ms} = -2\frac{\partial u_i^{r''}}{\partial x_j}\frac{\partial U_j}{\partial x_i}. \tag{23}$$

Solving Eq. (23) yields a relation between the mean-shear part of the pressure spectrum $\phi_p^{ms}(\boldsymbol{\kappa})$ and the vertical velocity spectrum $\phi_{33}(\boldsymbol{\kappa})$:

$$\phi_p^{ms}(\boldsymbol{\kappa}) = 4\left(\frac{\partial U}{\partial z}\right)^2 \frac{\kappa_1^2}{\kappa^4}\phi_{33}(\boldsymbol{\kappa}). \tag{24}$$

Assuming $\phi_p^{ms}(\boldsymbol{\kappa})$ is isotropic in the horizontal plane and integrating over κ_3 gives

$$E_h^{ms}(\kappa_h) = \left(\frac{\partial U}{\partial z}\right)^2 B\kappa_h^{-11/3} \tag{25}$$

for the inertial range. B depends on the two-dimensional vertical velocity spectrum E_h^w in the inertial range:

$$B = 1.4\, E_h^w \kappa_h^{5/3}. \tag{26}$$

Pressure spectra near the top of the surface layer ($z = 0.10\ z_i$) are shown in Fig. 1 for the free convective case and the convective case with shear. Both show evidence of $\kappa^{-7/3}$ behavior in the inertial subrange. The constant a_3 in the three-dimensional pressure spectrum, derived from the least-squares best-fit of these spectra and Eq. (10), is about 4.0 in each case. Our value is quite close to the value determined from the velocity structure function (3.59, George et al. 1984). In contrast, the LES results of Métais and Lesieur (1992) indicated a value of 2.6 for a_3, and direct numerical simulation results yielded 7.0-8.0 (Pumir 1994; Gotoh and Fukayama 2001). Using Eqs. (10) and (13), the equivalent constant a_1 in the one-dimensional pressure spectrum is about 1.7 (for $a_3 = 4.0$). The constants changed little with height throughout the mixed layer for our cases (not shown).

The analytical solution for the buoyant pressure spectrum (Fig. 1) falls below the inertial-subrange pressure spectrum in each of the two cases, suggesting that buoyancy effects are not important in the inertial subrange of our pressure spectra. Buoyancy effects are also not important for all but the smallest wavenumbers in the energy-containing range. For the mean-shear case (Fig. 1b), the mean-shear contribution is larger than the buoyancy contribution, but still considerably smaller than the pressure spectrum in the inertial subrange.

For both cases, the Coriolis and subgrid-scale contributions determined from the Poisson solver were negligible (not shown). Since the buoyancy and mean-shear contributions are relatively small as well, we are left with the turbulence-turbulence term as the largest contributor in the inertial subrange. This would seem to be a necessary condition for a universal pressure spectrum in the inertial range.

4. PRESSURE-DIFFERENCE SPECTRA

We are especially interested in the behavior of pressure fluctuations near the surface. LES does not perform optimally there, however, because the horizontal scale of the vertical velocity field w decreases as we approach the surface. This causes the vertical velocity to be underresolved there and as a result the LES code relies more heavily than usual on its subgrid-scale model. The effect of this on the turbulent pressure field is unknown.

To assess the fidelity of the pressure spectra near the surface, we examine the behavior of differences in pressure at two near-surface heights. The idea is as follows. If p_1 and p_2 are random variables, the average of their squared difference is given by

$$\overline{(p_1 - p_2)^2} = \overline{p_1^2} + \overline{p_2^2} - 2\overline{p_1 p_2},$$

where $\overline{p_1 p_2}$ is the covariance of p_1 and p_2. If p_1 and p_2 are uncorrelated, $\overline{p_1 p_2}$ is zero and the difference vari-

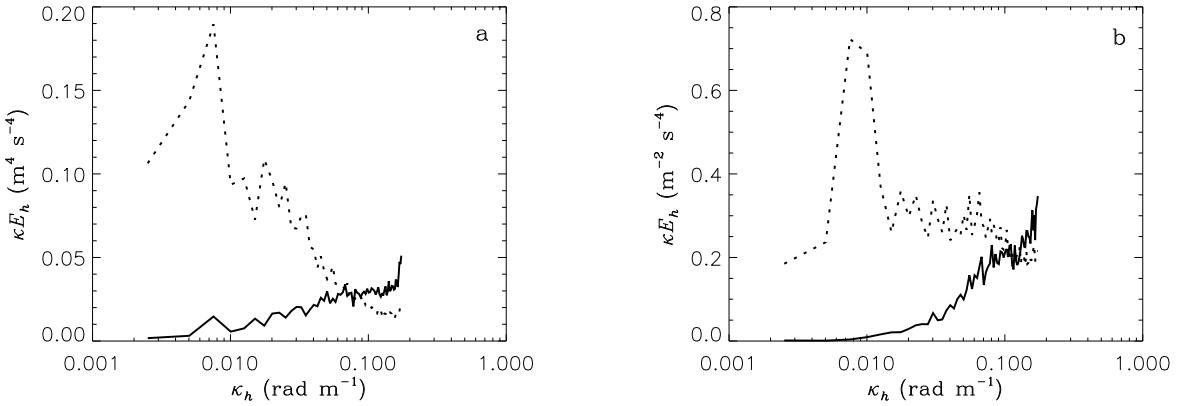

Figure 2: Two-dimensional pressure spectra (dotted line) and vertical pressure difference spectra (solid line) at $z = 0.02\ z_i$ for a) free convection and b) convection with shear.

ance is the sum of the variances. Conversely, if p_1 and p_2 are perfectly correlated, their difference variance is zero. Since the spectrum of a variable is the variance as a function of wavenumber, difference spectra can be interpreted in a similar manner.

At the largest wavenumbers in the LES (corresponding to the smallest resolved spatial scales, on the order of the LES grid mesh), the horizontal scale of the eddies is on the order of one-tenth of the boundary-layer depth. The correlation of the pressure at this wavenumber at vertical levels separated by that distance should approach zero, and thus the spectrum of the difference of pressure at the two vertical levels should approach the sum of the spectra of the pressure at the two levels. At the smallest wavenumbers (corresponding to the largest scales), the horizontal scale of the eddies is of the order of the boundary-layer depth. Thus the correlation of the pressure at nearby levels should approach 1.0, leading to very small values for the difference spectrum.

The vertical pressure-difference spectra and the pressure spectra (the latter at the lower of the two levels) are shown in Fig. 2 for $z = 0.02\ z_i$. The difference was calculated between the pressures at levels separated by three times the vertical resolution. For both the free-convection case (Fig. 2a) and the shear case (Fig. 2b), the difference spectra behave as expected in that the variance is high for large wavenumbers and near zero for small wavenumbers. The wavenumber at which the difference spectra cross the pressure spectra, an indicator of the wavenumber at which the decorrelation becomes significant, is about 0.1 rad m^{-1}, corresponding to eddies on the order of one-tenth of the boundary layer depth. Similar values are found throughout the mixed layer for both cases (not shown).

The results suggest that the pressure spectra in the energy-containing range are well-behaved even very close to the surface, with the errors caused by inadequate spatial resolution impacting mainly the smaller rather than the energy-containing scales.

5. SUMMARY

These LES results suggest the pressure field is well resolved for the two convective cases we present. Even close to the surface the pressure spectra exhibit $\kappa^{-7/3}$ behavior and the pressure difference spectra are well behaved. We also relate the inertial range constants of one-, two-, and three-dimensional pressure spectra.

Acknowledgments. This work is supported in part by the National Center for Physical Acoustics (under Subcontract #01-11-021).

REFERENCES

George, W. K., P. D. Beuther, and R. E. A. Arndt, 1984: Pressure spectra in turbulent free shear flows. *J. Fluid Mech.*, **148**, 155–191.

Gotoh, T., and D. Fukayama, 2001: Pressure spectrum in homogeneous turbulence. *Phys. Rev. Lett.*, **86**, 3775–3778.

Hill, R. J., and J. M. Wilczak, 1995: Pressure structure functions and spectra for locally isotropic turbulence. *J. Fluid Mech.*, **296**, 247–269.

Lumley, J., and H. Panofsky, 1964: *The Structure of Atmospheric Turbulence.* Wiley-Interscience, 239pp.

Métais, O., and M. Lesieur, 1992: Spectral large-eddy simulation of isotropic and stably stratified turbulence. *J. Fluid Mech.*, **239**, 157–194.

Moeng, C.-H., 1984: A large-eddy-simulation model for the study of planetary boundary layer turbulence. *J. Atmos. Sci.*, **41**, 2052–2062.

Moeng, C.-H., and J. C. Wyngaard, 1986: An analysis of closures for pressure-scalar covariances in the convective boundary layer. *J. Atmos. Sci.*, **43**, 2499–2513.

Pumir, A., 1994: A numerical study of pressure fluctuations in three-dimensional, incompressible, homogeneous, isotropic turbulence. *Phys. Fluids*, **6**, 2071–2083.

Wyngaard, J. C., 2002: *Concepts of Turbulence. Part 3: Statistical representation of turbulence*, 62pp.